Available online at www.sciencedirect.com
ScienceDirect
Computers and Mathematics with Applications 55 (2008) 132–148
An International Journal
computers & mathematics
with applications
www.elsevier.com/locate/camwa

Study of the collision of one rapid sphere on 3D packings: Experimental and numerical results

L. Oger*, M. Ammi, A. Valance, D. Beladjine

Groupe Matière Condensée et Matériaux, UMR CNRS 6626, Université de Rennes I, 35042 Rennes Cedex, France

Received 8 November 2006; accepted 5 April 2007

Abstract

We report on experimental studies of the collision process between an incident bead and a three-dimensional packing of mono-size beads. The understanding of such a process and the resulting ejection of grains is, in particular, crucial to describe aeolian sand transport. We present here recent experimental results on the collision and ejection process when varying the angle and the speed of the incident bead. We performed numerical simulations of one bead collisions on the surface of a static granular medium. The simulations have been done for two and three dimensional packings of beads. The effects of the incident bead velocity, the shot angle, the mechanical parameters and the packing structure are analyzed for ordered and disordered 2D packings but only disordered 3D packings. The 2D results are in good agreement with available experimental data. The 3D simulations give good preliminary results about the shock wave propagation through the stacking and provides new insights in the ejection process ("splash function").

Keywords: Granular transport; Saltation; DEM modelisation

1. Introduction

The transport and collision of granular materials are very important in many fields, like pneumatic transport in civil engineering, grain breakage in pharmaceuticals, dune displacement in geophysical studies.... Despite this crucial role, they are far from well understood, and the manipulation of granular media is the cause of many problems. In the present paper, we focus on the problem of the collision of an incident bead with a static granular packing. This problem is, in particular, of great importance in the aeolian sand transport [1]. Indeed, the aeolian transport of sand involves collisions between energetic grains (accelerated by the wind) and the static sand bed. The understanding of this collision process appears to be crucial in order to predict the sand transport rate.

We investigate numerically the collision process for two-dimensional and three-dimensional packings. However, we restrict ourselves to the case where the incident bead and those from the packing are identical (equal in size and mass, and identical constitutive material). The collision process involving an incident bead much bigger and much heavier than the beads of the packing exhibits completely different features, leading to crater formation [2], and is

* Corresponding author. Tel.: +33 02 23 23 56 58; fax: +33 02 23 23 67 17.
E-mail address: luc.oger@univ-rennes1.fr (L. Oger).

0898-1221/$ - see front matter © 2007 Elsevier Ltd. All rights reserved.
doi:10.1016/j.camwa.2007.04.001

beyond the scope of our study. A typical collision results in the rebounding of the incident bead and the ejection of additional beads from the granular packing. We analyze, for two-dimensional and three-dimensional packing, the features of the collision process (rebound velocity of the incident bead, number of ejected beads, ejection speed) as a function of the speed and angle of the impacting bead, the nature of the packing (ordered versus disordered) and the variable mechanical parameters. This work is also performed in conjunction with Pasini and Jenkins [3], who study aeolian transport close to the surface of dunes and have to investigate in their statistical model a realistic 3D "*Splash*" function. The main outcomes of our numerical studies follow. In Section 4, we present the previous experimental and numerical results concerning the collision between an incident bead and a granular packing. In Section 3, we describe our mechanical model based on the Discrete Element Method. The experimental data are detailed in Section 4. In Section 5, we investigate the case of the three-dimensional packing impacted by a incident bead.

2. Review of previous experimental and numerical results

Most previous studies about the collision process of a single bead onto a static granular packing have been developed in the context of the aeolian sand transport. Such a transport involves collisions between energetic grains and the static granular bed. These energetic grains, termed "saltating grains" [1], move by successive jumps, alternatively bouncing on the granular bed and being accelerated by the wind. At each impact, additional grains are ejected from the granular bed and contribute to the over whole transport. The knowledge of the dynamic response is crucial for the future definition of the "*Splash*" function which can be described as the spatial and temporal distribution of moving beads due to an impact with one incident bead having a given velocity and direction. Bagnold [1,4] was the first to identify the importance of the collisional processes in aeolian sand transport and to analyze them.

2.1. Experimental results

Following Bagnold's works, several experimental studies focusing on the collision process have been conducted. Willets and Rice [5] have observed the collision phenomena with sand grains in wind tunnel experiments by means of high speed video recordings. They found that the impacting grains hit the sand surface at small angles between 10° and 16° and rebound with an angle varying between 20° and 40°. In addition, they established that the grains ejected from the granular bed have an average speed of one order of magnitude less than the impacting speed.

In parallel, model experiments of collision between an incident bead and a granular packing have been performed by different authors. Mitha et al. [6] studied the collision between a steel bead and a three-dimensional packing of steel beads. Beads of 4 mm diameter were used, and the impacting bead was launched at a speed of 20 m/s. They investigated essentially the influence of the impact angle on the collision process. They defined the normal restitution coefficient for the impacting bead as the ratio of the vertical rebounded velocity to the vertical incident one ($e_z = V_{rz}/V_{iz}$ with V_{iz}, the vertical component of the incident speed V_i and V_{rz} the vertical component of the bead velocity V_r after the collision). They found that e_z decreases with the impact angle ($e_z = 0.7$ at 17° and $e_z = 0.3$ at 31°). Furthermore, they showed that the number of ejected beads does not vary significantly when the impact angle increases from 17° to 31° and that the average vertical speed of ejection is of order of $3\sqrt{gd}$ where g is the gravitational acceleration and d the bead diameter. Werner [7] also studied extensively the collision process for shallow impacting angles ($\alpha_i \approx 15°$). He used sand grains and designed a special apparatus to propel a sand grain with a given velocity. He found in particular that the normal restitution coefficient for the impacting bead is independent of the incident speed ($\bar{e}_z(\alpha_i = 15°) = 0.82$). He observed, in addition, that the number of ejected grains increases with increasing incident speeds, and their vertical velocity distribution is nearly independent of the incoming bead's velocity.

More recently, Rioual et al. [8–10] designed a two dimensional set-up to investigate the collision between an incident bead and a two-dimensional granular packing where the beads were confined between two parallel vertical glass walls. One of his purposes was to study the influence of the packing size and structure (ordered versus disordered) on the collision process. They showed in particular that, in case of ordered packings, the mean number of ejected beads is very sensitive to the packing height (it increases with decreasing packing height). This effect has been attributed to the translation order through the packings. Indeed, the shock wave generated by the impact can propagate through the system along its symmetry axis without much dissipation; it can therefore reach easily the system boundaries and be reflected toward the packing surface, leading to the ejection of additional grains. In contrast, for disordered packings

where the translation order vanishes at a short distance, the mean number of ejected grains is much less sensitive to the packing size. Rioual et al. [10] also showed that the mean number of ejected beads is greater for disordered packings than for ordered ones of the same size. However, the mean vertical ejection velocity does vary significantly with the packing structure. Finally, they confirmed Werner's observations [7] that the normal restitution coefficient for the impacting bead e_z is independent of the impacting speed, and that the mean number of ejected grains varies nearly linearly with the impacting speed. However, unlike Werner's results [7], they found that the mean vertical ejection velocity increases slightly with increasing incident speed, and they proposed the following law for the distribution function of vertical ejection velocities (the denomination of the velocity terms is extended to V_e for the ejected bead velocity and V_{ez} for its vertical component) [9]:

$$P_{ej}(V_{ez}) = DV_{ez} \exp\left(-\frac{V_{ez}^2}{2\sigma^2}\right) \tag{1}$$

where $\sigma^2 = 0.1V_i\sqrt{gd}$ and $D = 1/\sigma^2$.

2.2. Numerical results

In addition to the experiments, some simulations of the collision process have been performed [11–13]. All of these numerical studies treated only the two-dimensional case. We present below the significant results of the main numerical studies. Werner [11,7] made two-dimensional simulations for the ordered packing of beads using a discrete element method. The interaction forces between particles have been modelled as follows. The normal force is described as a stiff damped oscillator and the shear force as well, except it is limited by the usual friction force. Werner simulations confirmed his experimental results. In particular, he was able to extract a law for the normal restitution coefficient for the impacting bead e_z, which is independent of the impacting speed:

$$\bar{e}_z(\alpha_i) = \left(\frac{0.320}{\sin\alpha_i} - 0.236\right) \times \bar{e}_z(15^\circ) \tag{2}$$

with α_i is the incident angle defined between the horizontal surface and the shooting direction and $\bar{e}_z(15^\circ)$ is equal to the value previously defined. He also established a law for the mean number N_{ej} of ejected particles as a function of the incident angle and speed:

$$\bar{N}_{ej}(\alpha_i, V_i) = 3.36\,\sin(\alpha_i) \times (0.572\,V_i - 0.915)\,. \tag{3}$$

In addition, he pointed out the importance of the geometry of the packing surface on the ejection process. Anderson and Haff [12,13] also performed extensive simulations of the collision of spherical bead onto a two-dimensional disordered packings. They investigated the influence of the impact velocity on the ejection process for shallow impacting angles (8° and 11°). They found that the mean number of ejected grains scales as

$$\bar{N}_{ej}(V_i) = 0.437V_i^{1.3} \tag{4}$$

and that the distribution of the velocities for the ejected beads (V_e) can be fitted by an exponential law

$$P_{ej}(V_e) = \frac{1}{0.25V_i^{0.3}} \exp\left(-\frac{V_e}{0.25V_i^{0.3}}\right). \tag{5}$$

The latter result is in contradiction with Werner's experimental results [7], which show that the distribution of ejection speeds is independent of the impact speed. Finally, they have determined the distribution of the rebound velocity V_r of the impacting bead which can be fitted by a Gaussian distribution:

$$P_r(V_r) = \frac{p_r}{\sqrt{2\pi}0.31V_i} \exp\left(-\frac{(V_r - 0.56\,V_i)^2}{2(0.31\,V_i)^2}\right) \tag{6}$$

with p_r representing the probability of rebound of the impacting bead: $\int_{-\infty}^{+\infty} P_r(V_r)\mathrm{d}V_r = p_r$ ($p_r = 0.95[1 - \exp(-2.\,V_i)]$).

3. Description of the numerical simulation

We present the different steps of the numerical simulations to mimic the collision process between an incident bead and a packing of identical beads. In order to save time of computation, we have simplified the technique to create the static packings of disks or spheres prior to the active part of the simulation. So in our numerical model, we perform two consecutive and complementary steps: a geometric piling step, and then a dynamic one.

3.1. Initial conditions and numerical implementation for the static packing generation

In the first step, we are doing a geometrical packing of particles in which the particles are just touching each other. From a mechanical point of view, this stage corresponds to a packing of perfectly rigid, frictionless grains. In order to generate the 2D or 3D packings that will then be used as starting points for the shooting study, we employed the Powell's algorithm [14]. Particles were placed inside a square (cubic in 3D) container. The first layer of beads are taken to a large initial size distribution (especially in the 2D disordered case) in order to avoid some long range order in the packing. Then each new particle was placed when its stability was obtained from 2 (or 3 at 3D) contacts on randomly chosen particles from all the highest previously placed ones. This technique generates perfectly disorder and dense packings [15,16]. The total number of disks or spheres used for the immobile packing is between 10,000 and 15,000 in two dimensions (150 large by 100 height) and 20,000 and 30,000 in three dimensions (43×43 on base by 16 layers). The initial size disorder for the first layer is then eliminated in order to be back to the assigned size distribution.

3.2. DEM model: Soft model approach

Our mechanical model is similar to the two-dimensional formulation of Savage [17]. The particles are modelled as disks or spheres according to the study (2D or 3D respectively). The mechanical and numerical model is exactly the same for both cases. The ith particle is characterized by its radius $\mathbf{r_i}$, and the position of its center (x_i, y_i and z_i if needed). A "soft-particle" approach is used, where each particle can have multiple contacts that can persist for extended durations. The size of the time step is chosen so that about 50 time steps elapse over a typical "rapid" collision. Both normal and tangential forces develop at the contact between two particles. The normal and tangential contact forces increase as the centers of the particles approach each other.

The normal force F_n at the contact is modelled as viscoelastic. It consists of an elastic (a linear spring) contribution and viscous damping (a linear dashpot) contribution, described as follows:

$$\begin{array}{ll} \text{compression:} & \\ F_n = K_n\delta - b_n v_n & \text{for } \delta = (\sigma - |\mathbf{r_i} - \mathbf{r_j}|) > 0 \\ \text{tension:} & \\ F_n = 0 & \text{for } \delta < 0 \end{array} \tag{7}$$

where K_n is the spring constant for normal forces, δ is the relative normal displacement between the centers of the two particles in contact, σ is the distance vector between the two centers, $\mathbf{r_i}$ and $\mathbf{r_j}$ are the two radii of the particles, v_n is the relative normal velocity, and b_n is the dashpot constant for normal forces. The force in the tangential direction is modelled also as a viscoelastic one; a linear spring and a linear dashpot are used to generate a tangential contact force as follows

$$F_t = K_t\delta_t - b_t v_t \tag{8}$$

where K_t is the spring constant for tangential forces, δ_t is the relative lateral displacement during the entire duration of the contact, v_t is the relative tangential velocity, and b_t is the dashpot constant for tangential forces. The tangential force, F_t is also limited to a maximum value, which is chosen according to a Coulomb friction law when slipping can occur, $F_t = \mu_i F_n$, where μ_i is the intergrain coefficient of friction. The tangential force acts in a direction opposite to that of the relative tangential velocity v_t. For this mechanical model, the time step calculation remains constant.

It is convenient to cast the governing Eqs. (7) and (8) in a non dimensional form and perform the computations based upon these dimensionless equations [17]. It is straightforward to revert back to physical variables if desired. Hence, all lengths are nondimensionalized by D, the diameter of the largest sized particles used in the computations.

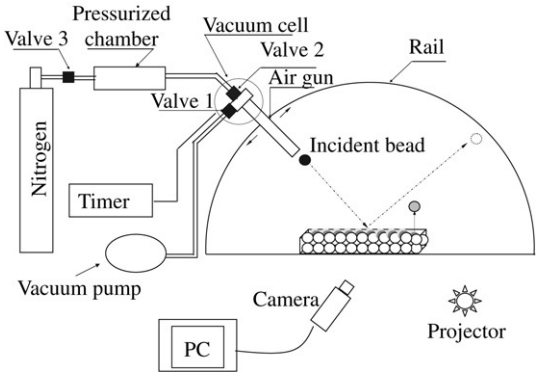

Fig. 1. Experimental setup.

Time is nondimensionalized by dividing by $\sqrt{M/K_n}$, where M is the mass of the largest particle and K_n the effective spring constant used in Eq. (7). Velocities are nondimensionalized by dividing by $D/\sqrt{M/K_n}$. Thus we introduce the following non dimensional time and spatial coordinates

$$(\tilde{t}, \tilde{x}, \tilde{y}) = \left(t\sqrt{\frac{K_n}{M}}, \frac{x}{D}, \frac{y}{D} \right). \tag{9}$$

Then all the conditions are defined to make a loop calculation of the force interactions between overlapping particles. For each particle, the forces acting on it are calculated; then the particle is displaced according to the resultant of all these forces. In order to decrease the global calculation time, the list of the neighboring particles is updated every 50 time steps. Local displacements of each particle are recorded.

3.3. Physical characteristic values

From a practical point of view, it is now necessary to assign to each disk some mechanical parameters. We choose those corresponding to the beads used in the collision experiment of Rioual et al. [8]. The disk or sphere diameter is taken equal to 6 mm and the weight is 0.2 g. The coefficient of restitution and the friction coefficient will be selected according to the desired studies (inside a range of 0.75–0.95 and 0.2–0.4 respectively) by adjusting the value of b_n. The spring constant K_n is chosen equal to 10^9 N m^{-1}, $K_t = 0.3K_n$ and $b_t = 0.5\,b_n$. The boundaries of the problem are defined as follows: the lateral walls (2 or 4 depending on the problem dimension) are defined as perfectly rigid but frictional. The bottom wall is defined as a flat frictional wall. A first period of the run permits a settling of the particles in order to obtain a dense disordered packing of particles in contact (to compensate the first step of the program which does not allow the grain overlaps). Indeed, the gravity has to be switched on before the shooting part of the simulation in order to densify and reorganize the packing. Then the shot particle is launched and the collision process proceeds. At each time step of the process, position and velocity of the particles are recorded.

4. Experimental results

4.1. Experimental set-up

We used PVC beads of 6 mm diameter for our experiments. The incident particle and those of the packing are identical. The friction and normal restitution coefficients of the bead are 0.19 and 0.91 respectively. The beads of packing were displayed randomly in a square box of dimension $42 \times 42 \times 23$ cm. The upper surface of the packing is leveled after each collision. The experimental set-up is shown in Fig. 1. An air gun has been designed to propel a single bead onto the packing. By varying the pressure, one can tune the incident speed of the bead (see [8] for a detailed description). The air gun can move on a semi-circular rail, which allows one to vary the incident angle from 0° to 90°. The collision process is recorded via a fast video camera which takes up to 1000 images per second. The video camera has been placed perpendicularly to the incident plane. The collision process utilizes two quite distinct scales of time,

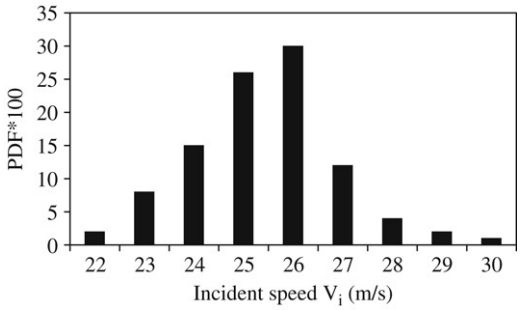

Fig. 2. Typical distribution of incident speed.

one corresponding to the movement of the incident bead and the other with the movement of the ejected beads (the rebound bead is characterized by high speed in comparison with the ejected beads). We have chosen a frequency of 500 Hz adapted to follow the movement of the incident bead and the ejected bead.

4.2. Image analysis

Consecutive images of the collision are analyzed to extract the cinematic properties of the incident bead and the ejected ones. The procedure is as follows. We first identify the ejected beads on each image of the video and determine their positions. Then we reconstruct the trajectories of each ejected particle and deduce their velocities. It is worth noting that the video images correspond to a projection of the 3D process onto the incident plane. Therefore we have only access to the vertical velocity V_z and the horizontal one V_x in the incident plane.

Furthermore, one should point out that the identification of the ejected beads is delicate in the first stages of the ejection process, when they are not clearly detached from the bed. As a consequence, we were able to identify the ejected beads only if they reached a height at least greater than one bead diameter above the bed. It means that we did not take into account, in our analysis, the weakly energetic beads which have a vertical ejection speed smaller than $\sqrt{2gd}$. The velocity of the incident bead is changed by modifying the air pressure in the pressurized chamber; however, for a given air pressure, the impact speed fluctuates. In this case the impact speed is measured a posteriori on the pictures of the collision, and then we plot this distribution to choose the collision corresponding to each value of the speed. Fig. 2 shows a typical example of the distribution of the incident velocity for one pressure.

We present here experimental results about the collision process with different incident speeds and impact angles. The impact angle is measured with respect to the horizontal (Fig. 3). We made two series of experiments: one at a given incident velocity of 26 m/s with various impact angles from 10° to 90°, and the other one at a fixed impact angle of 10° with incident speeds ranging from 18 to 40 m/s. To obtain good statistics, we carried out about 100 collisions for each set of impacting parameters (i.e., angle and velocity).

4.3. Properties of the rebound bead

As it has been described by Mitha [6] and Rioual [8], one can observe, in a the typical collision, the rebound of the incident bead and the ejection of some beads of the bed. The rebound bead is characterized by a much higher speed than for the ejected bead ones. We showed the effect of the impact angle and incident velocity in the properties of the rebound angle (rebound angle and restitution coefficient).

4.4. The effect of the impact angle

Angle of rebound: We plotted in Fig. 4 the mean rebound angle according to the impact angle. This curve shows that, for the large angles, the incident bead rebounds with an angle almost equal to impact angle, and for the grazing angles it is higher than the impact angle. The rebound angles of the incident bead do not vary with the incident speed (Fig. 5). For the impact angle of 10°, the incident bead rebounds, on average, with the angle of 22°.

Restitution coefficient: We introduce three different coefficients of restitution to characterize the rebound bead: $e_x = V_{rx}/V_{ix}$, $e_z = V_{rz}/V_{iz}$ and $e = V_r/V_i$, where V_i and V_r are respectively the incident and the rebound

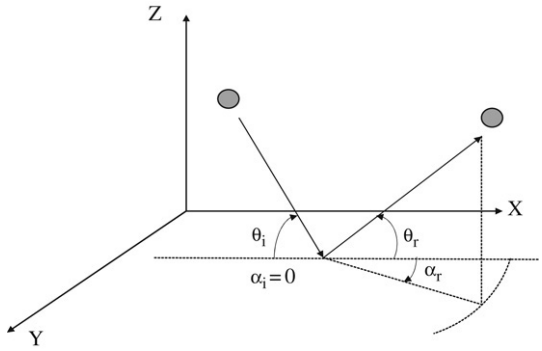

Fig. 3. Definition of rebound angle.

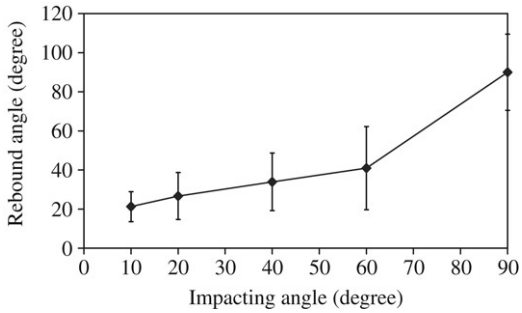

Fig. 4. Variation of the rebound angle with the impact angle. The impacting velocity is 26 m/s.

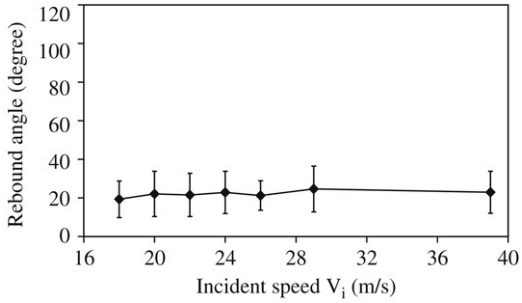

Fig. 5. Variation of the rebound angle with the incident speed V_i. The incident angle is 10°.

velocities, V_{ix} and V_{rx} are their horizontal components in the incident plane, and V_{iz} and V_{rz} correspond to their vertical components. We plotted, in Fig. 6, the evolution of the restitution coefficients e_x, e_z and e as a function of the impacting angle for a given incident speed of 26 m/s. We can notice a decrease of the restitution coefficients with increasing impact angle. Several comments follow. First, the incident bead dissipates much more energy for normal impacts [$e(90°) = 0.22$] than for grazing ones [$e(10°) = 0.78$]. Second, the vertical restitution coefficient e_z is found to exceed unity for grazing angles [$e_z(10°) = 1.55$]. This result does not violate energy conservation (since e is always smaller than 1), but simply means that a great part of the horizontal momentum of the incident particle is transferred to the vertical direction after the impact.

In the context of aeolian transport sand, this last result is of significant importance. Indeed, the sand grains transported by the wind in deserts have grazing impact angles between 8° and 15° [1,18,19]. This means that the latter will be able to rebound at a height at least equivalent to that before the collision. As a consequence, they will be able to continue their saltation process.

The variation of the vertical restitution coefficient with the impact angle has been also observed in 3D collision experiments by Mitha [6] and in 2D simulation by Werner [7]. From his simulation results, Werner proposed the

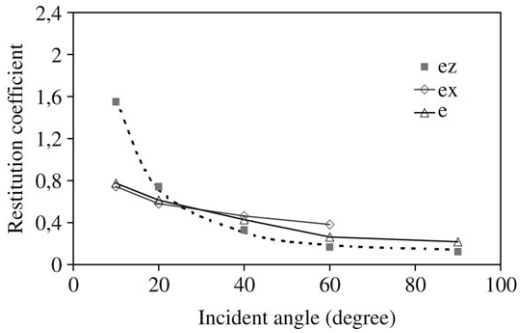

Fig. 6. Variation of the restitution coefficients e_z, e_x and e as a function of the impact angle. The impacting velocity is 26 m/s. The dashed line corresponds to the Werner's law fit.

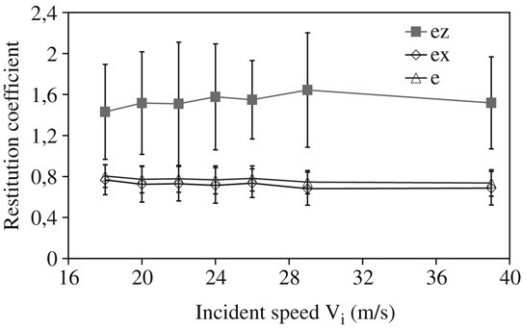

Fig. 7. Variation of the restitution coefficients e_z, e_x and e with the impact speed V_i. The incident angle is 10°.

following law for e_z:

$$e_z(\theta_i) = \frac{A}{\sin(\theta_i)} - B.$$

We tried to fit our data with this law and obtained a reasonable agreement. The best fit gives $A = 0.3$ and $B = 0.16$ (cf. the dashed line in Fig. 6).

We plotted in Fig. 7 the restitution coefficients e_x, e_z and e as a function of the incident velocity. We do not observe any significant variation of the restitution coefficients even if we increase the impact velocity by a factor 2. This independence with the incident velocity was also found in 2D collision experiments [8] and 3D ones with sand grains [7].

4.5. Properties of the ejected beads

When the incident bead impacts the bed, it not only rebounds but ejects other beads from the packing too. The ejected beads fly off in all directions (see Fig. 8) with a speed which rarely overcomes 10% of the incident velocity. We present below the features of the ejected beads when varying the impacting angle and incident velocity. We investigated the influence of the impact angle and the incident speed on the properties of the rebound bead. We recall that, for the angle effect we varied the impact angle from 10° to 90° at a given incident speed of 26 m/s. For the speed effect, the impact angle has been fixed at 10°, and the incident speed is varied between 18 and 39 m/s.

Number of ejected beads: In Fig. 9 we plotted the mean number of ejected beads per collision as a function of the impact angle. We note that the number of ejected beads increases with increasing impact angles. It seems one reaches a plateau for impacting angles greater than 40°. Oger et al. [22] found that the number of ejected beads increase with the impact angle (between 10° and 60°). We find the same evolution for the same angles. The average number of ejected beads as a function of the impacting speed is plotted in Fig. 10. This curve shows that the number of ejected beads increases linearly with the impacting speed. In addition, one can extrapolate from our data a speed threshold

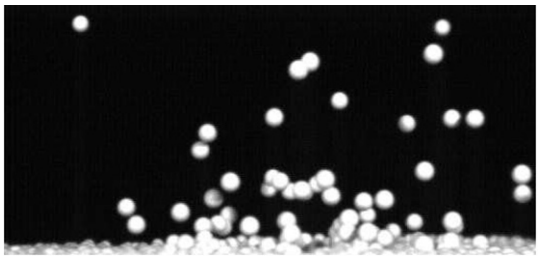

Fig. 8. Snapshot of the collision a few milliseconds after the impact.

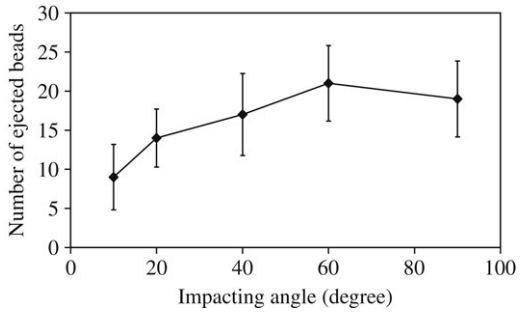

Fig. 9. Variation of the number of ejected beads N_{ej} with the impact angle θ_i. The incident speed is 26 m/s.

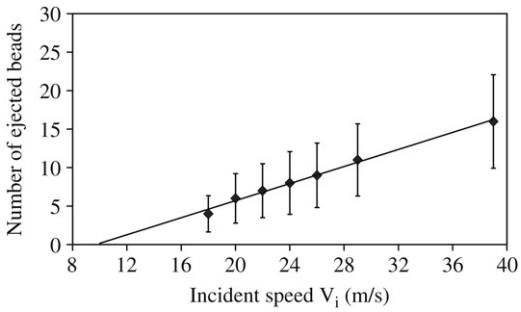

Fig. 10. Dependence of the impacting speeds on the number of ejected beads N_{ej}. The incident angle is 10°.

(V_i^{th}), below which there is no bead ejection. We find $V_i^{\mathrm{th}} \simeq 10\,\mathrm{m/s}$ or $V_i^{\mathrm{th}} \simeq 40\sqrt{g\,d}$. We can therefore propose the following law for the number of ejected beads:

$$N_{\mathrm{ej}} = p_1(V_i - V_i^{\mathrm{th}})$$

with $p_1 \simeq 0.55\,\mathrm{s/m}$. We recall that these fitting parameters have been obtained in the case of collisions with an impact of 10°. Additional experiments are therefore needed to determine how they vary with the impact angle. From the results of the previous section, one expects that p_1 and V_i^{th} increase with increasing impact angles. The linear increase of the number of ejected beads with the impact speed is in agreement with the preceding numerical and experimental studies performed in two dimensions [8,7].

Velocity of ejected beads: We studied the vertical speed distribution of the ejected beads; this distribution is capital for the splash function. In the aeolian sand transport, the vertical speed of ejection is very important. The grain, ejected at a high speed, will be able to reach the superior layers where the air speed is significant. In Fig. 11, we show the distribution of the vertical recoil speeds for various impact angles. We can note that all distributions collapse into a single master curve. The average of the vertical ejection speed V_z, as the Fig. 13 shows, is independent of the impact angle. Fig. 12 shows the distribution of the vertical ejection speeds for different impacting speeds. One notes that all distribution curves almost collapse into a single curve. This means that the distribution law, and consequently the mean

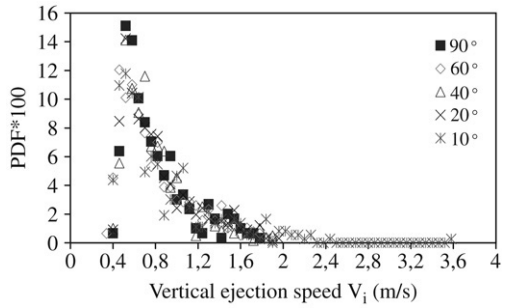

Fig. 11. Vertical ejection speed distribution for different impact angles. The distributions are normalized by the total number of ejected beads. The incident speed is 26 m/s.

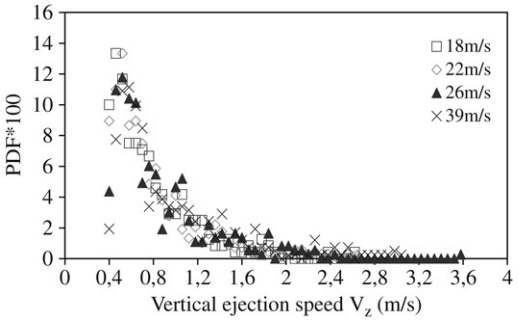

Fig. 12. Vertical ejection speed distribution for different impacting speeds. The distributions are normalized by the total number of ejected beads. The incident angle is 10°.

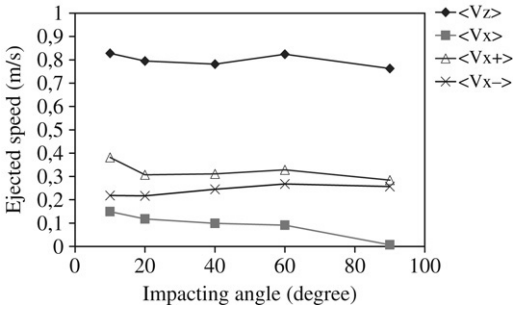

Fig. 13. Variation of the mean vertical ejection speed $\langle V_z \rangle$ and the mean horizontal ejection speed $\langle V_x \rangle$ with the incident angle. The incident speed is 26 m/s.

vertical ejection speed, is, at first order, independent of the impact velocity. However, a more careful analysis shows that the mean vertical ejection speed slightly increases with increasing impacting velocity (Fig. 14). The increase rate is approximately linear. One can extract from our data the following law: $\langle V_z \rangle = V_{z\,\min} + p_2(V_i - V_i^{\text{th}})$ with $p_2 \simeq 0.01$ and $V_{z\,\min} \simeq 0.6\,\text{m/s}$. Among the ejected beads, one finds the beads ejected in the direction of the shooting and in the opposite direction. The horizontal speed V_x+ of the beads which are ejected in the direction of the shooting is significant. It varies very little with the impact angle (Fig. 13) and it is independent to the incident speed (Fig. 14). The arithmetic average of the horizontal velocity V_x decreases with the impact angle. It remains constant if we varied the incident speed.

Location of ejection: We define the distance of ejection as the distance between the impact point and the location of take-off of the ejected beads. In Fig. 15, we have plotted the distributions of ejection distances for different impact speeds. The width of the region concerned with the ejection is of the order of 10 beads in the direction of shooting, and 5 beads in the opposite direction. One can note that out of the impact zone, that the probability of ejection is

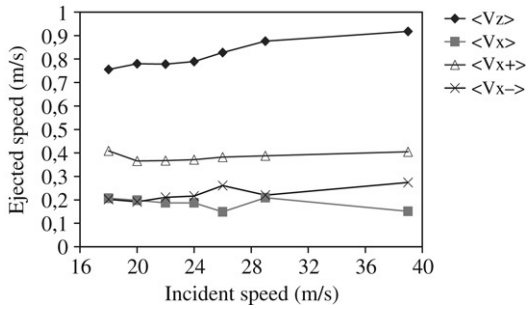

Fig. 14. Variation of the mean vertical ejection speed $\langle V_z \rangle$ and the mean horizontal ejection speed $\langle V_x \rangle$ as a function of the impacting speed. The incident angle is 10°.

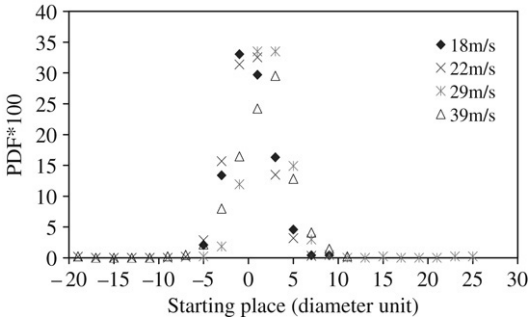

Fig. 15. Ejection distance distribution of ejected beads from impact point. The distributions are normalized by the total number of ejected beads. The incident angle is 10°.

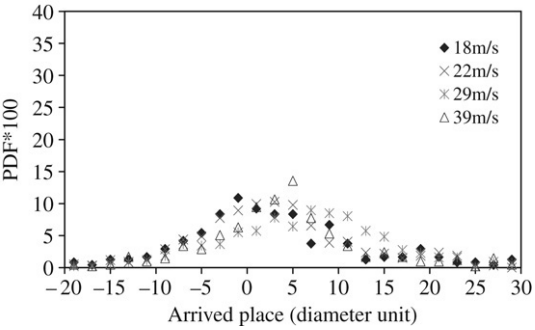

Fig. 16. Arrived distance distribution of ejected beads from impact point. The distributions are normalized by the total number of ejected beads. The incident angle is 10°.

almost negligible. The zone width does not seem to vary significantly with the impact speed. One sees that for small speeds (18 m/s, 22 m/s), the peak of the distribution is closer from the impact point. At 18 m/s, 33% of the beads eject before the impact point. For great speeds (29 m/s, 39 m/s), their peak is after and a little farther from the impact position. We have plotted, too, the distance distribution of the location landing (Fig. 16). We note that the peak of the distributions is near the impact point; this explains that many beads make small jumps. The beads which are ejected in the shooting direction have more energy. They make the great jumps and go to the distance of 235 beads.

4.6. Comparison with 3D simulation results

In this section, we compare our results with the numerical result of L. Oger. In general, the two results are qualitatively in agreement. For the incident bead, we compare the evolution of the rebound angle and the vertical restitution coefficient with the impact angle. The incident velocity, experimental and numerical, is respectively 26 m/s

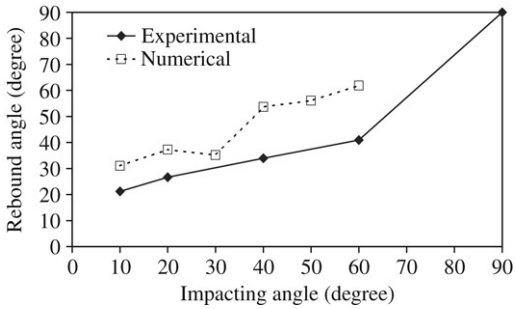

Fig. 17. Variation of the rebound angle with the impact angle. The impacting velocity is 26 m/s for the experimental curve and 30 m/s for the numerical curve.

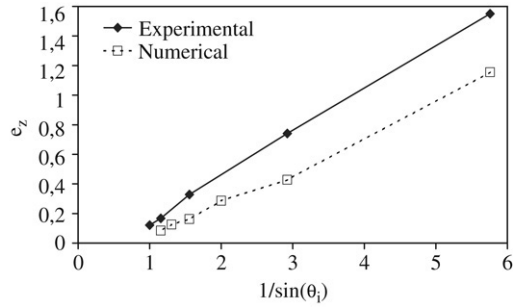

Fig. 18. Variation of the vertical restitution coefficient e_z with the impact angle. The impacting velocity is 26 m/s for the experimental curve and 30 m/s for the numerical curve.

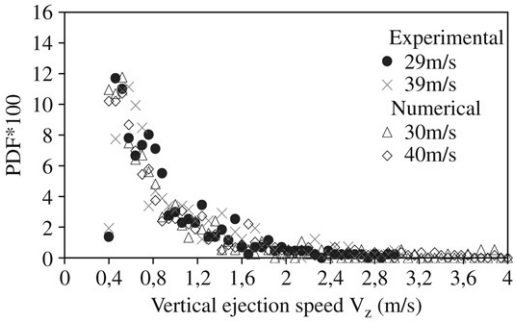

Fig. 19. Vertical ejection speed distribution for different impacting speeds. The distributions are normalized by the total number of ejected beads. The incident angle is 10°.

and 30 m/s. We find the same evolution of the rebound angle according to the impact angle (Fig. 17). The small difference can be explained by the value of restitution coefficient of the beads. It is higher in the simulation. In Fig. 18, we plotted the variation of the vertical restitution coefficient with the impact angle for the experimental and numerical results. We notice the same behavior for the two curves. In the numerical ones, the exact Werner's equation can be applied. The parameters of the experimental line are little different from Werner's. For the ejected beads, we compared the effect of the incident speed in the distribution of the vertical speed (for the incident angle of 10°). The distribution curves are superposed in the both cases (Fig. 19). There conform qualitatively.

5. Numerical simulations

The numerical study of the 3D collision is first motivated by the fact that experiments of collisions between an incident bead and a 3D packing are carried out in our lab, whose results will be published in the near future [20]. Second, all previous numerical simulations have been performed in 2D although the collision process is truly 3D.

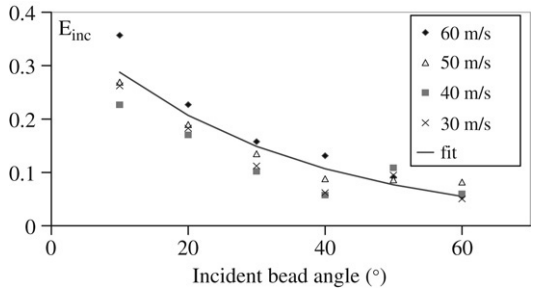

Fig. 20. Fraction of the energy conserved by the incident bead versus the impact angle for different impacting velocties. The continuous line corresponds to the best fit by an exponential law: $E_{\text{inc}} = 0.4 \exp(-0.1\alpha_i/3)$.

5.1. Description of the 3D numerical simulations

The disordered case can only be analyzed in a statistical manner. We need therefore to perform a large number of different runs for each set of given parameters. As the two dimensional analysis has shown that the collision process depends greatly on the impacting velocity and the incident angle, we have focused our attention on the modification of the collision by varying the angle and the velocity of the impacting particle. The use of disordered static dense packing allows us to choose an arbitrary vertical plane of incidence. Indeed, as the packing is expected to be horizontally isotropic, all vertical planes are equivalent for the collision process. This has been checked numerically by observing the homogeneous distribution on the azimuthal plane of all ejecta orientations.

In order to obtain a good statistical analysis, we have performed for each set of parameters (angle and speed) a few specific runs. We have generated up to *four* different dense disordered packings with 20 000 or 30 000 spheres (as already mentioned: 43 × 43 on base by 16 layers), and for each of them, we have launched at least *ten* beads impacting at different locations close to the center of the packing. This procedure give us a minimal number of ejected beads around 400 and a maximal close to 800, which are enough to extract good statistics. In this simulation, we have chosen an internal restitution coefficient equal to 0.9.

5.2. Analysis of the 3D results

The first issue of our work is to confirm the main results obtained in the three dimensional experiments (Section 4). We will look successively at the results for the incident bead and the ejected ones.

5.2.1. Results for the incident bead

In Fig. 20, we have plotted E_{inc} versus the impact angle for different impacting speeds. We observe a clear decrease of E_{inc} with the impact angle. This confirms the results obtained in 2D. In addition, one can note that E_{inc} is not sensitive to the impacting speed except for grazing angle (around 10°).

It can be interesting to replot the previous data in terms of the vertical restitution coefficient $e_z = V_{rz}/V_{iz}$ in order to check the Werner's law (Eq. (2)). In Fig. 21, we represent e_z versus $1/\sin(\alpha_i)$ for different impacting speeds. All data collapse onto Werner's prediction. The dash line is obtained from Eq. (2) with exactly the same parametric values (in particular with $\bar{e}_z(15°) = 0.82$). The good agreement between the two dimensional simulations of Werner [11,7] and our three dimensional ones is quite surprising. We are still investigating this point in order to understand the main information behind this fact.

In order to describe the properties of the rebound bead, we need to investigate how the rebound angle varies with the impact angle. Fig. 22 presents an average value of the angle of rebound versus the incident angle. We can imagine that the roughness of the surface tends to increase the dispersion of angles of rebound. An asymptotic value around 22° seems to appear for very small angles and has to be compared to the observation made by Willets and Rice [5]. This angle can be related to the roughness of the surface. Indeed, if we assume that the surface has the same packing fraction as the inner part of the packing (around 64% of fraction), the mean distance between the beads can be obtained (1.1 radius). A minimal number of three neighbors can maintain one sphere, so it can be ejected if it can pass on top of its neighbors, and so a basic calculation of the direct angle for this geometrical configuration gives easily an angle around 22°.

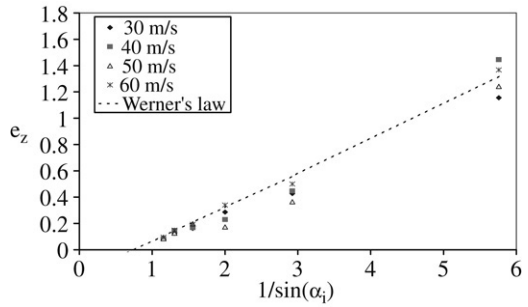

Fig. 21. Vertical restitution coefficient for the incident bead versus $1/\sin(\alpha_i)$. The continuous line corresponds to the Werner's law (see Eq. (2)).

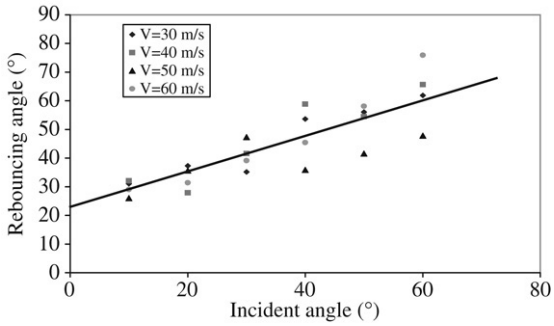

Fig. 22. Evolution of the angle of the rebound for the incident bead versus the shot angle for impacting velocities.

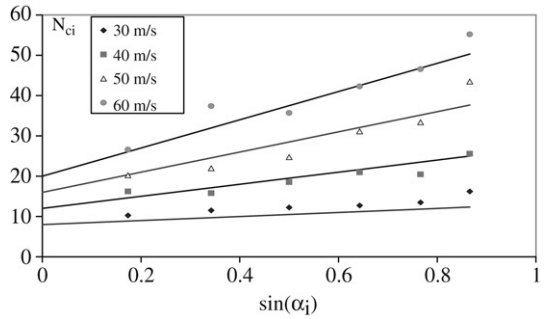

Fig. 23. Evolution of the number of ejected beads versus impact angle for different impacting velocities. The continuous lines correspond to the following fit: $N_{\text{ej}} = (0.4V_i - 4.0) + (V_i - 25.0) * \sin(\alpha_i)$.

5.2.2. *Results for the ejected beads*

Let us now analyze the features of the ejectas. We have observed from both experimental [8] and numerical two dimensional studies and our preliminary three dimensional experiments [21], that the number of ejected beads increases linearly with the incident bead velocity. Our 3D simulation confirms this feature. We also find that the number of ejectas N_{ej} slightly increases with increasing impact angle. Fig. 23 illustrates these results; we have plotted the number of ejectas versus the impact angle for different impact velocities. Our data are well fitted by $N_{\text{ej}} = (0.4V_i - 4.0) + (V_i - 25.0) * \sin(\alpha_i)$.

In order to fully describe the *Splash* function, we have analyzed the kinetic energy of the ejectas. We have found that the fraction of energy transferred to the ejectas E_{eject} is almost independent of the impacting velocity, but decreases linearly with the impact angle from 0.06 to 0.03. The same feature is observed for the fraction of vertical energy gained by the ejectas ($E_{\text{vert\_eject}}$), but the values decrease such as E_{inc} in Fig. 22 from 0.08 down to 0.01. We observed that the evolution of the energy fraction transferred to the ejected beads is almost constant around 4% for E_{eject} and

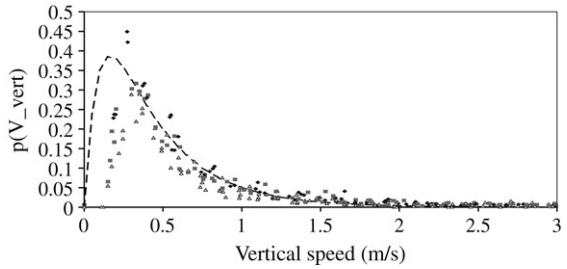

Fig. 24. Probability distribution of the vertical ejection velocities for the ejected beads for different shooting angles and impacting velocities. Each symbol corresponds to a given impacting velocity (△: 30 m/s, □: 40 m/s, ⋄: 50 m/s) with different shot angles between 10° and 60°. The dash line corresponds to the best fit for $\alpha = 1.6$ and $\beta = 0.4$.

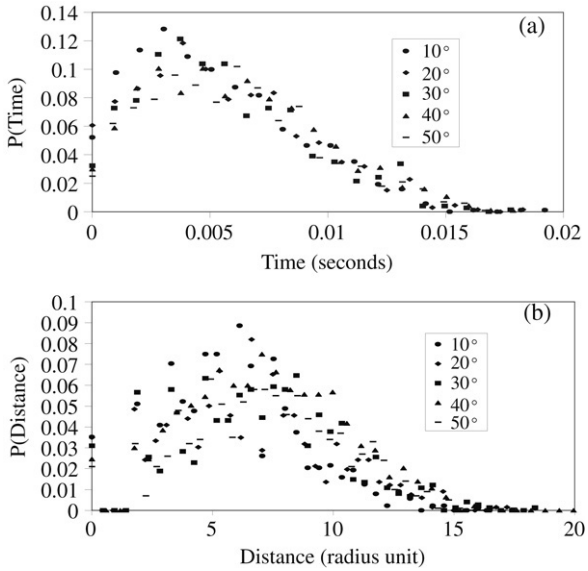

Fig. 25. Probability distribution of the ejection time of the ejectas (a) and of the ejection location (measured from the impact point) for various impact angles (10°–50°) and a given impacting velocity of 50 m/s.

around 1.5% for $E_{\text{vert\_eject}}$ for the angles and velocities investigated so far. This result implies that the total (rebound bead and ejected beads) released energy decreases with the impact angle. This fact confirms why the saltation process occurs more easily with grazing angles, and why the constant aeolian transport of sand is mostly possible for a small number of grains.

We have also investigated the distribution of the vertical ejection speed of the ejectas (Fig. 24) for different impacting velocities and different impact angles. All data seem to collapse onto a single master curve. This means that to characterize the ejectas, it is enough to know the number of ejected grains N_{ej} for each set of impact parameters (angle and velocity of the shot) plus the form of this "universal" distribution curve. We have tried to fit this curve by an exponential law of the form $V_{ez}^{\alpha} \exp\left[-\frac{V_{ez}^{\beta}}{A\sqrt{gd}}\right]$, but without success. As we have defined a threshold altitude for the detection of the ejected beads, we cannot evaluate and take into account the amount of beads having very small vertical velocities, so it is not possible to find a good fit for both small and large vertical speeds.

Let us analyze now the take-off times of the ejectas and their locations of ejection. Fig. 25 represents the distribution of the take-off times of the ejectas (a) and that of their ejection location (b) for different impact angles and an impacting velocity of 50 m/s. Note that the origin of time is taken to be the moment of the shot impact, and that the location of ejection is measured in terms of distance from the impact point. One clearly sees that both distributions are insensitive to a change of the impact angle and that they have similar shape. These last results seem to indicate that there is a correlation between the time and location of ejection.

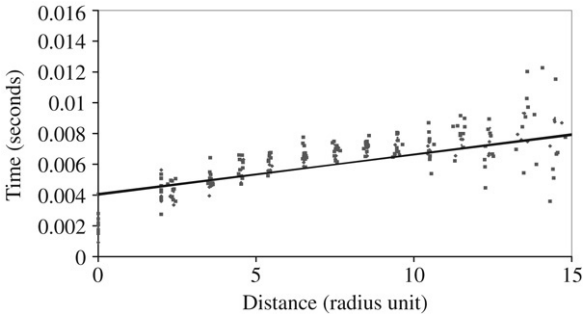

Fig. 26. Take-off time of ejected beads versus ejection distance from the impact point for shooting angle varying from 10° to 60° and velocities comprised between 30 and 60 m/s. Each point corresponds to an individual ejected bead.

To check this, we have plotted, for each of the individual ejectas, their take-off times versus their ejection distances from the impact point for different impact angles and impacting velocities (Fig. 26). One notes a clear linear correlation between these two quantities. This correlation is linked to the propagation of the shock wave induced by the impact. The slope of the linear interpolation of the data should give an order of magnitude for the wave speed ($\approx$24 m/s). Some preliminary experimental experiments give us a range of values around 5 m/s which is not too far from our results. Note that as the mechanical properties of the packings do not change from one simulation to one another, it is not surprising to observe that the wave speed is almost constant in the range of the impacting bead velocity.

In a complement to the previous analysis, it is important to note that a great part of the incident energy is dissipated inside the packing: only 10% to 30% of the incident energy is released through the rebound bead and the ejectas. It is very difficult to quantify and analyze the local dilation and propagation of the shock wave inside the packing.

5.3. Summary of results

The quasi universalities of the probability distributions of the vertical ejection velocities, and the take-off times and the ejection distances of the ejectas are quite surprising, but are of great interest for the theoretical modeling approach. If we try to conjugate all the information obtained from these 3D numerical simulations, only a few characteristics are needed to fully describe the *Splash* function. First, it is found that grazing impacts allow that the rebound bead conserves a great part of the incident kinetic energy. Second, the individual features of the ejected beads (ejection velocities, take-off time and ejection distance) do not depend on the angle and speed of the incident bead. Their features are more or less universal. Only the number of ejected beads is controlled by the impact kinetic energy and impact angle. A small amount of these displaced grains get high enough (vertical velocity higher than 1 m/s) to be transported by the wind, the rest only roll or slide on the surface of the dunes, but participate nevertheless in the sand transport.

6. Conclusion

We have seen that the Discrete Element Method applied to the determination of the *Splash* function for the two and three dimension configurations is very powerful. We get a good correspondence between the numerical results and experimental results in the 2D case. The next step will be to validate our 3D simulations by a thorough comparison with the recent experiments of Beladjine et al. [20]. Preliminary comparisons with these experimental results are good and very encouraging.

We should point out the great perspective offered by the numerical simulations, which allow easy variations of the mechanical properties of the beads and the geometry of the packings over a large range of parameter variations. In particular, simulations will be very helpful for improving the description of the *Splash* function in the case of multiple impacts. Indeed, in the context of aeolian sand transport, one expects that, for high wind speeds, the description of the impact processes of the saltating grains in terms of independent single collisions breaks down. It would be then interesting to investigate how the *Splash* function might be modified in the case of multiple collisions.

References

[1] R.A. Bagnold, The Physics of Blown Sand and Desert Dunes, Methuen, London, 1941.
[2] A.M. Walsh, K.E. Holloway, P. Habdas, J.R. de Bruyn, Morphology and scaling of impact craters in granular media, Physical Review Letters 91 (2003) 104301–104304.
[3] J.M. Pasini, J.T. Jenkins, Aeolian transport with collisional suspension, Philosophical Transactions of the Royal Society (2004).
[4] R.A. Bagnold, The shearing and dilatation of dry sand and the 'singing' mechanism, Proceedings of the Royal Society of London A 295 (1966) 219–232.
[5] B.B. Willets, A. Rice, Collisions in aeolian saltation, Acta Mechanica 63 (1986) 255.
[6] S. Mitha, M.Q. Tran, B.T. Werner, P.K Haff, The grain-bed impact in aeolian saltation, Acta Mechanica 63 (1986) 267.
[7] B.T. Werner, A steady-state model of wind blown sand transport, Journal of the Geological Society 98 (1990) 1–17.
[8] F. Rioual, A. Valance, D Bideau, Experimental study of the collision process of a grain on a two-dimensional granular bed, Physical Review E 62 (2000) 2450–2459.
[9] F. Rioual, Ph.D. Thesis, Unversity of Rennes 1, 2002.
[10] F. Rioual, A. Valance, D Bideau, Collision process of a bead on a two-dimensional bead packing: Importance of the inter-granular contacts, Europhysics Letters 61 (2) (2003) 194–200.
[11] B.T. Werner, P.K. Haff, The impact process in aeolian saltation: Two-dimensional simulations, Sedimentology 35 (1988) 189.
[12] R.S. Anderson, P.K. Haff, Simulation of eolian saltation, Science 241 (1988) 820.
[13] R.S. Anderson, Wind modification and bed response during saltation of sand in air, Acta Mechanica 1 (Suppl.) (1991) 21–51.
[14] M.J. Powell, Computer-simulated random packing of spheres, Powder Technology 25 (1980) 45–52.
[15] D. Bideau, A. Gervois, L. Oger, J.-P. Troadec, Geometrical properties of disordered packings of hard disks, Journal de Physique 47 (1986) 1697–1707.
[16] L. Oger, J.-P. Troadec, D. Bideau, J.A. Dodds, M.J. Powell, Properties of disordered sphere packings i. geometric structure: Statistical model, numerical simulation and experimental results, Powder Technology 46 (1986) 121–131.
[17] S.B. Savage, Disorder, diffusion and structure formation in granular flows, in: D. Bideau, A. Hansen (Eds.), Disorder and Granular Media, North Holland, Amsterdam, 1993, pp. 255–287.
[18] B.R. White, J. Schulz, Magnus effect in saltation, Journal of Fluid Mechanics 81 (1977) 497–512.
[19] R.S. Anderson, B. Hallet, Sediment transport by wind: Toward a general model, Geological Society of America Bulletin 97 (1986) 523–535.
[20] D. Beladjine, M. Ammi, A. Valance, L. Oger, 3d collision process between an incident bead and a granular packing, Physical Review E 75 (2007) (in press).
[21] D. Beladjine, A. Valance, M. Ammi, L. Oger, Experimental and numerical study of the collision between an incident bead and a three dimensional granular packing, in: S. McNamara, H.J. Herrmann (Eds.), Powders and Grains 2005, Balkema, 2005.
[22] L. Oger, M. Ammi, A. Valance, D. Beladjine, Discrete Element Methods to study the collision of one rapid sphere on 2D and 3D packings, The European Physical Journal E 17 (2005) 467–476.